PCCP

^{31}P nuclear spin singlet lifetimes in a system with switchable magnetic inequivalence: experiment and simulation

Journal:	*Physical Chemistry Chemical Physics*
Manuscript ID	CP-ART-07-2021-003085.R1
Article Type:	Paper
Date Submitted by the Author:	16-Aug-2021
Complete List of Authors:	Korenchan, David; New York University, Chemistry Lu, Jiaqi; New York University, Chemistry Levitt, Malcolm; University of Southampton, School of Chemistry Jerschow, Alexej; New York University, Chemistry

ARTICLE

^{31}P nuclear spin singlet lifetimes in a system with switchable magnetic inequivalence: experiment and simulation

Received 00th January 20xx,
Accepted 00th January 20xx

DOI: 10.1039/x0xx00000x

David E. Korenchan[a], Jiaqi Lu[a], Malcolm H. Levitt[b], and Alexej Jerschow*[a]

^{31}P NMR spectroscopy and the study of nuclear spin singlet relaxation phenomena are of interest in particular due to the importance of phosphorus-containing compounds in physiology. We report the generation and measurement of relaxation of ^{31}P singlet order in a chemically equivalent but magnetically inequivalent case. Nuclear magnetic resonance singlet state lifetimes of ^{31}P pairs have heretofore not been reported. Couplings between ^{1}H and ^{31}P nuclei lead to magnetic inequivalence and serve as a mechanism of singlet state population conversion within this molecule. We show that in this molecule singlet relaxation occurs at a rate significantly faster than spin-lattice relaxation, and that anticorrelated chemical shift anisotropy can account for this observation. Calculations of this mechanism, with the help of molecular dynamics simulations and *ab initio* calculations, provide excellent agreement with the experimental findings. This study could provide guidance for the study of ^{31}P singlets within other compounds, including biomolecules.

Introduction

In nuclear magnetic resonance (NMR) spectroscopy, information can often be encoded and then stored in protected magnetization modes. Nuclear spin singlet states could potentially allow for extended information storage, although the conditions facilitating long lifetimes are not always easy to predict.

Since the first demonstration in 2004 of generating long-lived NMR singlet order in organic molecules in solution[1, 2], there has been considerable interest in the study of singlet states in various compounds, and we wish to point to recent comprehensive reviews describing the relevant NMR theory and progress in the field[3-6]. For a two spin-1/2 system, one may write the triplet and singlet states in terms of the spin states as follows:

$$|T_1\rangle = |\uparrow\uparrow\rangle \qquad |T_0\rangle = \frac{1}{\sqrt{2}}(|\uparrow\downarrow\rangle + |\downarrow\uparrow\rangle) \qquad |T_{-1}\rangle = |\downarrow\downarrow\rangle$$

$$|S_0\rangle = \frac{1}{\sqrt{2}}(|\uparrow\downarrow\rangle - |\downarrow\uparrow\rangle)$$

These states can be populated in such a way that singlet order (SO) is overpopulated from its equilibrium value. SO can be written as

$$\mathrm{SO} = |S_0\rangle\langle S_0| - \frac{1}{3}\sum_{m=-1}^{+1}|T_m\rangle\langle T_m|$$

Once populated, SO relaxes to its equilibrium value with a time constant that can significantly differ from T_1. For example, SO between ^{13}C nuclei in a $^{13}C_2$-labeled naphthalene derivative in degassed and deuterated acetone at 0.4 T has been reported to have a lifetime of 70 min, representing a 60-fold increase over T_1 relaxation[7]. SO has been utilized in a variety of applications, including measurements of slow flow and diffusion[8] or molecular rearrangement[9], determination of molecular geometry[10, 11], spectral isolation of desired protein or metabolite moieties[12-14], and storage of hyperpolarized magnetization[15, 16]. Because SO can be difficult to generate and cannot be directly detected via the NMR coil, specialized chemical transformations[17, 18] and/or NMR pulse sequences have been designed to populate the singlet state and to subsequently convert it back to detectable magnetization. These conversion methods include the 'Sarkar' method[9], the magnetization-to-singlet/singlet-to-magnetization (M2S-S2M) sequence[15] and modified versions thereof[18-20], spin-lock induced crossing (SLIC)[21], and adiabatic-passage spin order conversion (APSOC) type[12, 22, 23] sequences. The choice of the conversion sequence and the level of conversion depend on the relative magnitudes of chemical shift differences and *J*-couplings, the expected bandwidth, the anticipated lifetimes, and inhomogeneities of both the main magnetic field (B_0) and the applied radiofrequency field (B_1)[20].

Most NMR singlet-state studies have involved pairs of ^{1}H, ^{13}C, and ^{15}N nuclei. Long-lived states of ^{19}F spins have recently been studied as well[24]. As the field of singlet-state NMR approaches biological study, there may be increasing interest in studying singlet states between ^{31}P nuclei. ^{31}P has a high natural abundance and is biologically prevalent, particularly in the form

[a] Department of Chemistry, New York University, New York, NY, USA.
[b] School of Chemistry, University of Southampton, Southampton, UK

Email: alexej.jerschow@nyu.edu

Electronic Supplementary Information (ESI) available: additional NMR spectroscopy data, including decoupled spectra and SLIC pulse sequence optimization results, details on molecular dynamics simulations, and information on R_1/R_s curve fitting. See DOI: 10.1039/x0xx00000x

of mono-, di-, or triphosphate groups attached to biomolecules. These ^{31}P nuclei tend to couple via scalar *J*-coupling with neighbouring spins (for example in polyphosphates); therefore, many biological molecules are likely to sustain ^{31}P NMR singlet order. It has been speculated that long-lived ^{31}P nuclear singlets could play a role in quantum effects within neuronal processes[25]. To date, there have not been any reported measurements of singlet state lifetimes of ^{31}P nuclei, in part perhaps because it is not straightforward to identify suitable molecules with weak inequivalence that would allow the generation and sustainment of SO in these compounds.

In this study, we therefore considered a case of chemical equivalence, but mild magnetic inequivalence that could be used to populate the singlet state and could also be switched off by decoupling[26]. The molecule tetrabenzyl pyrophosphate (TBPP) fits such requirements (Figure 1a). Another reason for this choice was that the time-averaged structure in solution may display a local inversion symmetry, a property known to enable particularly long singlet lifetimes[27]. Yet, as shown below, the lifetimes observed in this compound are surprisingly short. A combination of molecular dynamics (MD) and *ab initio* calculations is used to identify anticorrelated chemical shift anisotropy (CSA) as the primary mechanism responsible for these short lifetimes.

Materials and methods

Chemicals

Tetrabenzyl pyrophosphate was purchased from Sigma Aldrich (St. Louis, MO, USA). Deuterated chloroform ($CDCl_3$, 99.8% enrichment) was purchased from Cambridge Isotope Laboratories (Tewksbury, MA, USA). All NMR studies used a sample of TBPP dissolved in $CDCl_3$ at a concentration of 80 mM.

NMR experiments

All NMR experiments were performed using a Bruker 9.4T NMR spectrometer (400 MHz ^{1}H frequency) equipped with a double-tune, direct-detect NMR probe. The 90° pulse lengths for ^{1}H and/or ^{31}P were calibrated on the day of each experiment. All pulse sequences used a total repetition time of at least 5 times the maximum T_1. Standard pulse-acquire ^{1}H and ^{31}P NMR spectra were acquired using the following parameters: 8k complex points, 8 scans, 8 kHz spectral width, 1 s acquisition time, 1 Hz spectral resolution. The ^{31}P T_1 was measured using an inversion-recovery sequence with the same acquisition parameters except for a 4k spectral width and 4k complex points.

A spin-lock induced crossing (SLIC) pulse sequence[21] as shown in Figure 2a was used for singlet-triplet transfer optimization as well as singlet relaxation measurements. All SLIC pulse sequences included a zero-rank filtration sequence prior to the singlet-to-magnetization transfer pulse, as described in Tayler et al[28] and indicated in Figure 2a, using 11.1% of the maximum spectrometer gradient amplitude for the gradient pulses. This filter removed undesired rank-one and rank-two spin operators while preserving singlet order. A two-step phase cycle was also utilized, similar to that used by Kiryutin et al[12], in order to eliminate signal arising from z-magnetization excited by the second spin-lock pulse. Prior to singlet relaxation measurements, an optimization sequence was performed, in which the signal was measured as a function of both spin-lock pulse duration and amplitude. Acquisition parameters were the same as those listed in the preceding paragraph. A minimum delay of 1 ms was used in between the spin-lock pulse and the zero-rank filter. The optimal spin-lock pulse parameters were then used to measure singlet relaxation by incrementing the singlet relaxation delay. These experiments used the same acquisition parameters as above with the following exceptions: the spectral width was 4 kHz, and the number of complex points was 4k. Singlet relaxation measurements were also performed with continuous-wave irradiation during the singlet relaxation delay: 1000 Hz on the ^{31}P frequency and/or 300 Hz irradiation on either the methylene or phenyl ^{1}H resonance frequency.

For the low-temperature NMR experiments, the sample temperature was decreased using a liquid nitrogen evaporator (Bruker, Billerica, MA, USA). The sample temperature was calibrated over the entire temperature range using a pure methanol temperature standard.

Simulation

Simulation of NMR spectra was performed using the Spinach MATLAB package[29] (http://spindynamics.org/group/). Scalar coupling and chemical shift parameters were determined by minimizing the residual between simulated and experimental spectra using MATLAB's "fminunc" function. Both the ^{31}P and the ^{1}H spectra were fitted together to improve the convergence. The ^{1}H and ^{31}P peak linewidths were also fitted along with the parameters mentioned above. All ^{1}H peaks were assumed to have the same linewidth, and the same held for all ^{31}P peaks.

CSA tensor visualizations were performed with SpinDynamica v. 3.6 (pre-release version)[30] using the function Ovaloid (which was based on a procedure described previously[31, 32]). Molecular graphics were created using Mathematica's MoleculePlot3D function for the tensor visualization plot and VMD[33] for the molecular dynamics (MD) snapshot.

MD simulations were performed using Amber20[34]. The system was prepared in antechamber using the general Amber force field (GAFF). The molecule was prepared and solvated by $CHCl_3$ in an isotropic box of 50 Å size using Amber's antechamber and tleap programs. Following that, the system energy was minimized using 3000 steps with the steepest descent method and 2000 steps with the conjugate gradient method. Then the system was heated to the desired temperature in 20,000 steps using a Langevin thermostat with gamma_ln=5. Stabilization at the target temperature was performed at constant temperature (gamma_ln=5) and pressure, using a Berendsen barostat with a pressure relaxation time of 1 ps, for 100,000 steps. A short production run of 10,000 steps was performed using the NVE ensemble conditions.

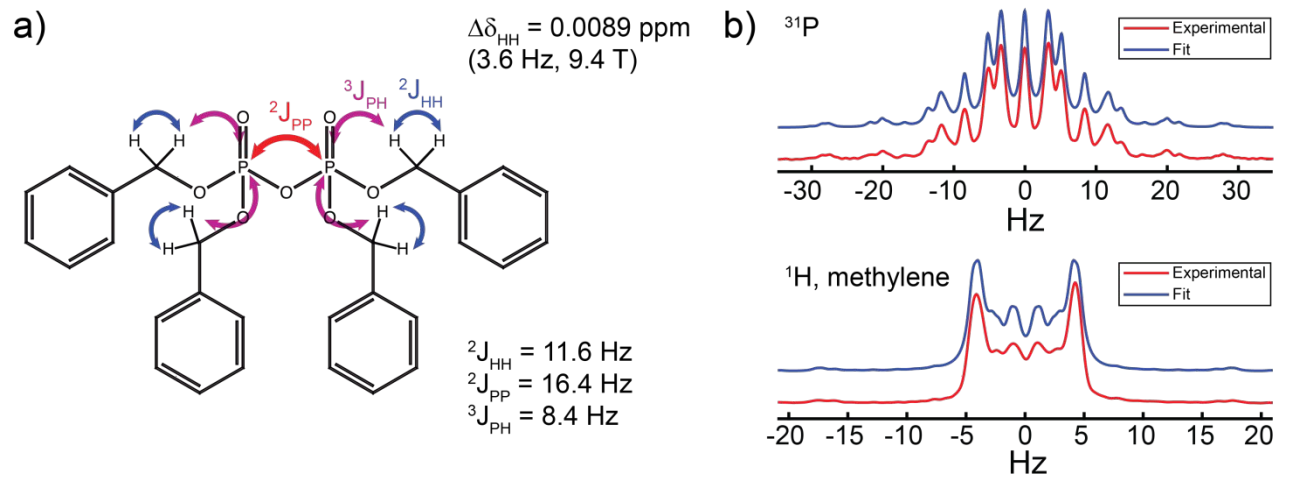

Figure 1 – Coupling patterns in tetrabenzyl pyrophosphate determined via spectral simulation. (a) Chemical structure of TBPP with indicated chemical shift differences and J-coupling constants. Each ^{31}P nucleus couples to four proximal ^{1}H nuclei three bonds away, as well as to one another. The ^{1}H nuclei on each methylene carbon are chemically inequivalent and therefore exhibit *J*-coupling to one another. (b) Simulated ^{31}P (top) and methylene ^{1}H (bottom) NMR multiplets overlaid on experimental data, using the chemical shift and coupling constants indicated in part (a).

Following that, a production run of 20 million steps was performed using Amber's GPU code (pmemd.cuda). A timestep of 0.2 fs and a cutoff of 11 Å for electrostatic interactions were used throughout. Periodic boundary conditions were used for heating, stabilization, and production, and the SHAKE algorithm for hydrogen bonds was used for stabilization and production. Stabilization and equilibration were checked by monitoring density, temperature, diffusion, and energy, which were found to remain close to equilibrium values.

Second rank correlation times were extracted from the production trajectories using the MDAnalysis package[35] for the P-P and P=O internuclear vector reorientation motion.

100 random conformations of the TBPP molecule were extracted from the trajectory. These conformations were equilibrated with Gaussian16 (using the B3LYP DFT functional with a 6-31G(d) basis set and implicit chloroform solvent) to find the local minimum in order to avoid overestimates of the tensors due to instantaneous vibrational or torsional excursions. 69 of these optimizations converged according to Gaussian's frequency calculation. CSA tensors were calculated for these converged conformations using the same functional/basis set combination.

The CSA tensors were then separated into their traceless symmetric and antisymmetric components. For the relaxation expressions, two types of averages of the tensor norms were calculated: (1) Individual tensor norm averages for spin-lattice relaxation rate (R_1) calculations; (2) the averages of the norms of the differences of the tensors of the two phosphate nuclei were calculated for the singlet state relaxation rate (R_S) calculations.

While CSA relaxation is often studied using only the symmetric part of the tensor, it is well known that the antisymmetric portion can contribute significantly to relaxation[7, 36, 37].

The expressions for the R_1 component calculations are

$$R_1^{sym} = \frac{2}{15}\left(\omega_0\sqrt{\frac{3}{2}}\|\sigma_{sym}\|_F\right)^2\frac{\tau_2}{1+(\omega_0\tau_2)^2} \quad (1)$$

$$R_1^{anti} = \frac{1}{6}(\omega_0\|\sigma_{anti}\|_F)^2\frac{\tau_1}{1+(3\omega_0\tau_1)^2} \quad (2)$$

Here, σ_{sym} and σ_{anti} designate the traceless symmetric and the antisymmetric tensor components, respectively, and $\|\sigma\|_F$ indicates the Frobenius norm of a tensor, i.e. the square root of the sum over the squares of all tensor elements. τ_2 is the second rank correlation time. For isotropic motion, one may assume that the first rank correlation time $\tau_1 = 3\tau_2$.

In the context of singlet-state relaxation, it was shown specifically that the antisymmetric component could become a major relaxation contribution[37]. In that work, the expressions for the R_S components were provided in the fast motion regime. Outside of that regime, the expressions become

$$R_S^{sym} = \frac{2}{9}(\omega_0\|\Delta\sigma_{sym}\|_F)^2\frac{1}{5}\left(2\tau_2 + \frac{3\tau_2}{1+(\omega_0\tau_2)^2}\right) \quad (3)$$

$$R_S^{anti} = \frac{2}{9}(\omega_0\|\Delta\sigma_{anti}\|_F)^2\frac{\tau_1}{1+(3\omega_0\tau_1)^2}, \quad (4)$$

where $\Delta\sigma_{sym}$ and $\Delta\sigma_{anti}$ represent the symmetric and the antisymmetric component of the difference between the tensors at the two phosphorus sites.

For the R_1 calculations, the correlation time for the P=O bond reorientation was used, and for the R_S calculation, the one for the P-P internuclear vector was used.

Data processing and analysis

The pulse-acquire and inversion-recovery NMR data were processed using Bruker TopSpin software. The SLIC pulse optimization data were read into MATLAB and processed using custom scripts. For the singlet relaxation experiments, spectra were processed and integrated in TopSpin and fitted to an exponential decay in MATLAB. Changes in singlet relaxation rate constant with ^{31}P or ^{1}H irradiation were calculated as percentage change relative to singlet relaxation without any irradiation at each temperature.

Results and discussion

Simulation of NMR spectra

Simultaneous fitting of both the ^{31}P NMR spectrum and the methylene ^{1}H NMR multiplet via spin system simulation provided further insights into the interactions between ^{31}P and ^{1}H nuclear spins within the TBPP molecule. The results of spectral fitting are displayed in Figure 1, along with the extracted values for the *J*-coupling constants. Excellent agreement between simulation and experimental results were obtained by modelling the TBPP molecule as each ^{31}P nucleus exhibiting 3-bond *J*-couplings to four ^{1}H nuclei on the methylene carbons nearby, as indicated in Figure 1a. The magnetic inequivalence is established by the differences in coupling constants between each ^{31}P nucleus to a given ^{1}H nucleus; in particular, the four ^{1}H on each side of the molecule couple to the nearby ^{31}P nucleus, but not to the ^{31}P on the opposite side of the molecule. Longer-range couplings to the phenyl protons appeared to be too small to be considered. A similar case of chemical equivalence and magnetic inequivalence has been reported previously between ^{13}C nuclei in diethyl oxalate[26]. The hypothesis that the J_{PH} couplings give rise to the magnetic inequivalence between ^{31}P spectra is further supported by the observation that the ^{31}P spectrum with ^{1}H decoupling gives rise to a singlet, rather than a doublet of doublets (Supplementary Figure S1a, ESI).

Another intriguing finding is that the ^{1}H nuclei on each methylene carbon are chemically inequivalent, with a chemical shift difference of 0.0089 ppm (3.6 Hz at 9.4 T). This finding suggests that the methylene ^{1}H pairs should also be able to sustain SO. This is confirmed by the observation that the ^{31}P-decoupled ^{1}H spectrum appears to be a strongly coupled doublet of doublets (Supplementary Figure S1b, ESI). Spectral fitting on this multiplet gave similar chemical shift and *J*-coupling parameters to those obtained via the simultaneous spectral fitting results shown in Figure 1b.

Optimization of singlet NMR parameters

The NMR simulation results suggested that ^{31}P SO between the two ^{31}P nuclei in the pyrophosphate moiety of TBPP could be populated. In order to characterize the ^{31}P SO, we performed an optimization of the spin-lock pulses utilized in the spin-lock induced crossing (SLIC) pulse sequence[21] (Figure 2a), in order to identify the optimal locking pulse length and amplitude. In the absence of relaxation, the optimal spin lock amplitude should be equal to the homonuclear *J*-coupling between nuclei, and

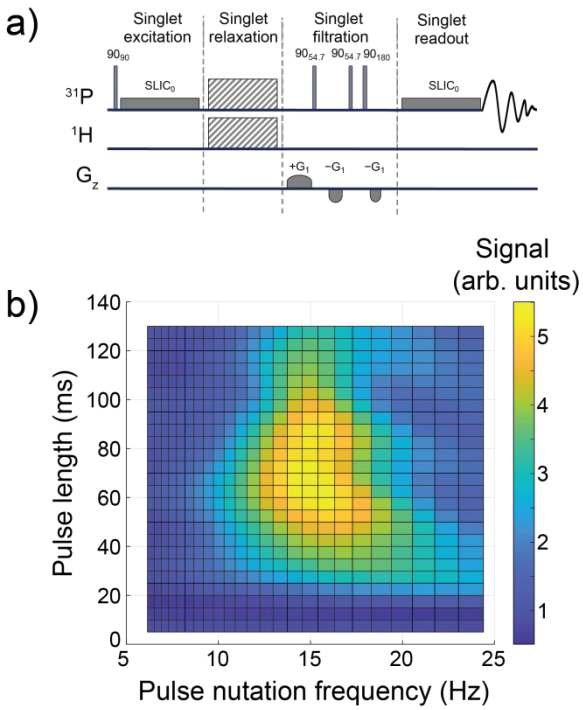

Figure 2 – Optimization of ^{31}P singlet generation for TBPP using the SLIC pulse sequence. (a) Schematic of the SLIC pulse sequence utilized in this study. Subscripts indicate relative pulse phases. Spin-lock (SLIC) pulses induce singlet-triplet transitions in order to prepare and read out the singlet state. A filtration sequence was utilized before the second spin-lock pulse to remove undesired spin coherences. Some experiments, such as those shown in Figures 3c and 5, included ^{31}P and/or ^{1}H decoupling, indicated with hatched-fill rectangles. (b) Spin-lock pulse optimization results. The signal arising from the singlet state is plotted in colour as a function of pulse length and nutation frequency.

the optimal pulse duration should be equal to $1/(\sqrt{2}\Delta\nu)$, where $\Delta\nu$ normally corresponds to the chemical shift frequency difference between the pair of spin-1/2 nuclei[21]. For our case, however, the inequivalence arises from the differences in ^{1}H-^{31}P J-coupling constants between each ^{31}P nucleus in TBPP. This has been observed to be the case when studying the NMR singlet of ^{15}N,^{15}N'-azobenzene, which also displays chemical equivalence and magnetic inequivalence, using the SLIC pulse sequence[38]. We therefore expected the optimal pulse length to relate to the value of $^{3}J_{PH}$ obtained by spectral fitting.

Figure 2b displays the signal arising from the singlet as a function of spin-lock pulse nutation frequency and duration. Singlet-triplet interconversion was maximized at a pulse nutation frequency of 14.6 Hz and a pulse length of 60 ms. The pulse nutation frequency matched well with the J_{PP} value of 17.3 Hz predicted by simulation. The optimal pulse duration, however, was shorter than anticipated, corresponding to a frequency of 11.8 Hz, using the equation in the preceding paragraph, rather than $^{3}J_{PH}$ = 8.4 Hz. It is possible that this discrepancy is due to singlet relaxation during the spin-lock pulse.

The optimal pulse nutation frequency and length did not deviate more than 5.4% and 7.7%, respectively, of the optimal values at room temperature over the whole temperature range (Supplementary Figure S2, ESI).

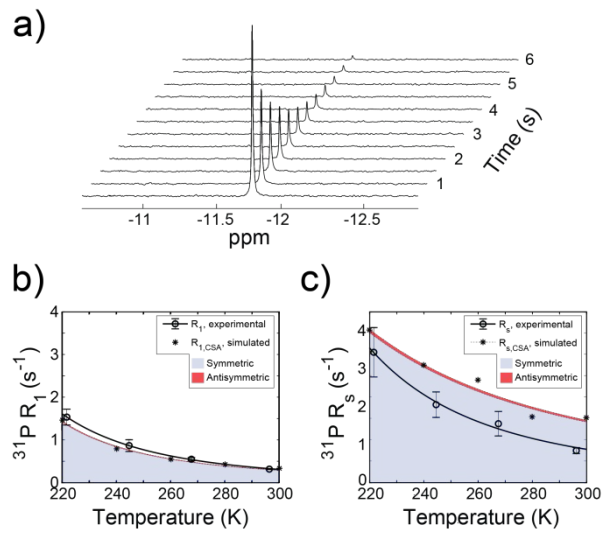

Figure 3 – Measurement and simulation of ^{31}P spin-lattice and singlet relaxation for TBPP. (a) Example stacked spectral plot of ^{31}P singlet order decay. ^{1}H decoupling was applied during acquisition. (b-c) ^{31}P relaxation rate constants of (b) longitudinal magnetization (R_1), and (c) singlet order (R_s), as a function of temperature. Experimental and simulated data are plotted on the same graph. Both ^{1}H and ^{31}P irradiation were applied during the singlet relaxation delay. The major relaxation contribution arises from the symmetric component of the CSA, and the antisymmetric portion is very small (red-filled area).

We also obtained further evidence that the TBPP ^{31}P singlet state is accessible via the J_{PH} couplings rather than a small ^{31}P chemical shift difference. When we performed the SLIC pulse optimization described above while applying decoupling at the methylene ^{1}H frequency during both spin-lock pulses, we observed a linear increase in the optimal spin-lock nutation frequency with increasing decoupling power, as well as a decrease in signal arising from the singlet at high decoupling powers (Supplementary Figure S3, ESI). Therefore, the *J*-couplings between ^{31}P and ^{1}H nuclei were identified as the main enablers of singlet-triplet conversion.

Measurement and simulation of ^{31}P spin-lattice and singlet relaxation

In order to characterize the longevity of ^{31}P SO, we compared measurements of the spin-lattice relaxation rate (R_1) and singlet relaxation rate (R_s). Figure 3a displays an example stacked spectrum of signal decay arising from the ^{31}P singlet. Surprisingly, the ^{31}P singlet of TBPP decayed 1.5-2 times faster than spin-lattice relaxation over a range of temperatures between 297 and 221 K (Figure 3b-c). We hypothesized that CSA might be the cause of this unexpected finding. We therefore performed molecular dynamics (MD) simulation to model the CSA-dependent ^{31}P relaxation of TBPP in $CDCl_3$ (Figure 4). In order to calculate R_1 and R_s relaxation rates according to Eqs. (1-4), we extracted correlation times from the MD trajectories and combined these with the CSA tensors obtained from *ab initio* calculations as described in the methods section. The average difference tensor norms were: 261.0 and 27.8 ppm for the symmetric and antisymmetric components, respectively. The standard deviations for these were found to be 7.7 and 9.2 ppm, respectively. A plot for the tensor norms for the tensors of all converged conformations is shown in Supplementary Figure S4. These calculations produced a very good

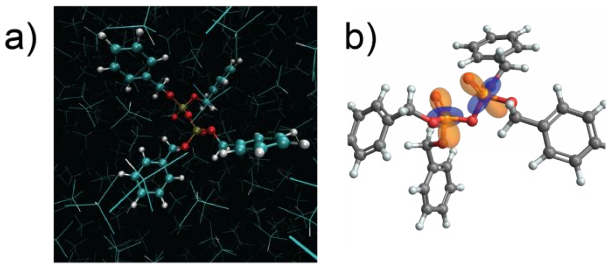

Figure 4 – (a) Snapshot of MD simulation structure of TBPP solvated in $CDCl_3$. (b) Representative snapshot with visualization of the symmetric portion of the CSA tensors.

correspondence with the experimental values for R_1, and a moderate overestimation of R_s values over the temperature range studied (Figure 3b-c). We therefore concluded that CSA was the dominant relaxation mechanism in TBPP, leading to a very short-lived singlet state. The intramolecular dipolar coupling mechanism (P-H couplings) can be estimated to be much smaller than the CSA contribution, and does not lead to shortening of the singlet lifetime with respect to R_1.

The observation of a very short singlet lifetime between the ^{31}P nuclei in the studied compound is quite different from many studies with other nuclei, where T_S is generally longer than T_1. Indeed, most relaxation mechanisms affecting T_1 do not influence the SO relaxation as strongly, including dipole-dipole couplings, scalar couplings and even interactions with paramagnetic species[4], where generally some degree of correlation exists. CSA, on the other hand, can cause stronger singlet relaxation than spin-lattice relaxation depending on the relative orientation of the CSA tensors of the two participating spins[10]. This situation appears to be the case for the significant shortening of singlet lifetimes in TBPP.

It has recently been shown that chemical exchange phenomena, such as reversible protonation, can induce singlet relaxation through modulation of isotropic chemical shifts[39]. We do not anticipate a significant contribution from this mechanism in the current study, since the solvent is aprotic.

As described above, CSA will not lead to singlet relaxation if the molecule exhibits inversion symmetry between the two spins[4]. Only the averaged structure of TBPP, however, displays some limited inversion symmetry, but none of the instantaneous conformers do. Upon examination of representative tensors, it was found that the major components of the tensors pointed along the P=O double bond. In all conformations examined, these bonds were not aligned for the two phosphorus nuclei (the second rank order parameter $\langle P_2(\cos\theta)\rangle$ for the relative angle was determined to be -0.2, corresponding to an angle of approximately 60°). This is due to the bridging oxygen bonds. Hence, a significant degree of anticorrelation of the tensors is observed, which is the source of the shortening of T_s.

Manipulation of singlet relaxation via spin irradiation

We investigated the effect of spin locking on the singlet relaxation rate by applying strong continuous-wave irradiation

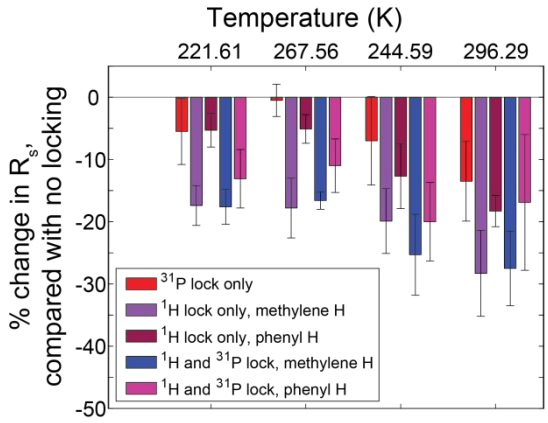

Figure 5 – Effects of radiofrequency irradiation on ^{31}P and ^{1}H resonances during singlet relaxation, as a function of temperature. All percentage changes in R_s are relative to R_s without locking at the respective temperature. Error bars represent standard deviation.

on ^{31}P and/or ^{1}H between triplet-to-singlet and singlet-to-triplet conversions. The ^{1}H irradiation frequency was set to either the methylene ^{1}H resonance or the phenyl ^{1}H resonance. In general, irradiation on either the ^{1}H or ^{31}P nuclei had a stronger effect on R_s at higher temperatures than at lower temperatures (Figure 5). Additionally, irradiating the methylene ^{1}H resonance produced a larger R_s decrease than irradiating either the phenyl ^{1}H resonance or the ^{31}P multiplet. Decoupling ^{1}H nuclei directly deactivates the singlet-triplet leakage relaxation pathway, and therefore it is expected that irradiating the more strongly coupled methylene protons will have the largest impact on lengthening the singlet lifetime. Applying a strong, 1000 Hz spin-lock to the ^{31}P spins produces a much weaker effect, and the reason is currently not understood.

Conclusions

We have reported the characterization of singlet order between two magnetically inequivalent ^{31}P nuclei within tetrabenzyl pyrophosphate. SO is accessed via the ^{1}H-^{31}P couplings, leading to magnetic inequivalence. We have also demonstrated that SO relaxes more quickly than longitudinal magnetization, and that the large CSA present within the compound is the primary relaxation mechanism. In particular, an anticorrelation of the tensors can be identified as the origin for these effects. Furthermore, the agreement between measured and calculated relaxation rates is very good, given the many assumptions that go into mimicking the solvated system with MD simulations, and the crudeness of extracting CSA tensors from snapshots via *ab initio* calculations.

These findings have important ramifications for the singlet-state lifetimes in other ^{31}P-bearing compounds, since relatively large CSA tensors are commonly found within phosphates and other biological molecules containing phosphorus. If CSA dominates the relaxation of singlet order within biological diphosphates, then this finding would suggest that exposure to a high magnetic field might cause phosphorus-based physiological effects of quantum processes[25] to become negligible. On the other hand, this result does not preclude the existence of such processes at low fields.

Author Contributions

D.E.K. contributions: conceptualization (helped define project scope), formal analysis (performed statistics), investigation (performed experiments), methodology (modified pulse sequences), software (wrote processing scripts, performed spectral optimization and parameter fitting), visualization (designed figures), writing – original draft, and writing – review & edit.

J.L. contributions: formal analysis (analyzed experimental data), investigation (performed experiments), and writing – review & edit.

M.H.L. contributions: supervision (interpretation of results, guidance with tensor visualization and parameter extraction), resources (provided relaxation expressions), and writing – review & edit

A.J. contributions: conceptualization (initial project idea + definition), formal analysis (analysis of relaxation data), funding acquisition, software (performed relaxation simulations and molecular dynamics and *ab initio* calculations, spectral optimization and parameter fitting), supervision, and writing – review & edit

Conflicts of interest

There are no conflicts to declare.

Acknowledgements

We acknowledge funding though an award of the U.S. National Science Foundation, award no. CHE 2108205, and an award by the Heising-Simons Foundation. AJ acknowledges the receipt of a Diamond Jubilee Visiting Fellowship to the University of Southampton. We thank Dr. Christian Bengs for extensive discussions on singlet relaxation mechanisms and critical reading of the manuscript. We further thank Dr. Mohamed Sabba for helpful and stimulating discussions on phosphorus relaxation mechanisms. This work was supported in part through the NYU IT High Performance Computing resources, services, and staff expertise (especially Dr. Shenglong Wang).

Notes and references

1. M. Carravetta, O. G. Johannessen and M. H. Levitt, *Phys Rev Lett*, 2004, **92**, 153003.
2. M. Carravetta and M. H. Levitt, *J Am Chem Soc*, 2004, **126**, 6228-6229.
3. M. H. Levitt, in *Encyclopedia of Magnetic Resonance*2010.
4. M. H. Levitt, *Annu Rev Phys Chem*, 2012, **63**, 89-105.
5. F. Teleanu, A. Sadet and P. R. Vasos, *Prog Nucl Magn Reson Spectrosc*, 2021, **122**, 63-75.
6. *Long-Lived Nuclear Spin Order: Theory and Applications*2020.

7. G. Stevanato, J. T. Hill-Cousins, P. Hakansson, S. S. Roy, L. J. Brown, R. C. Brown, G. Pileio and M. H. Levitt, *Angew Chem Int Ed Engl*, 2015, **54**, 3740-3743.
8. S. Cavadini, J. Dittmer, S. Antonijevic and G. Bodenhausen, *J Am Chem Soc*, 2005, **127**, 15744-15748.
9. R. Sarkar, P. R. Vasos and G. Bodenhausen, *J Am Chem Soc*, 2007, **129**, 328-334.
10. P. Ahuja, R. Sarkar, P. R. Vasos and G. Bodenhausen, *J Chem Phys*, 2007, **127**, 134112.
11. M. C. Tayler, S. Marie, A. Ganesan and M. H. Levitt, *J Am Chem Soc*, 2010, **132**, 8225-8227.
12. A. S. Kiryutin, A. N. Pravdivtsev, A. V. Yurkovskaya, H. M. Vieth and K. L. Ivanov, *J Phys Chem B*, 2016, **120**, 11978-11986.
13. S. Mamone, N. Rezaei-Ghaleh, F. Opazo, C. Griesinger and S. Gloggler, *Sci Adv*, 2020, **6**, eaaz1955.
14. S. J. Devience, R. L. Walsworth and M. S. Rosen, *NMR Biomed*, 2013, **26**, 1204-1212.
15. G. Pileio, M. Carravetta and M. H. Levitt, *Proc Natl Acad Sci U S A*, 2010, **107**, 17135-17139.
16. G. Pileio, S. Bowen, C. Laustsen, M. C. Tayler, J. T. Hill-Cousins, L. J. Brown, R. C. Brown, J. H. Ardenkjaer-Larsen and M. H. Levitt, *J Am Chem Soc*, 2013, **135**, 5084-5088.
17. Y. Zhang, X. Duan, P. C. Soon, V. Sychrovsky, J. W. Canary and A. Jerschow, *Chemphyschem*, 2016, **17**, 2967-2971.
18. B. Kharkov, X. Duan, E. S. Tovar, J. W. Canary and A. Jerschow, *Phys Chem Chem Phys*, 2019, **21**, 2595-2600.
19. C. Bengs, M. Sabba, A. Jerschow and M. H. Levitt, *Phys Chem Chem Phys*, 2020, **22**, 9703-9712.
20. B. Kharkov, X. Duan, J. W. Canary and A. Jerschow, *J Magn Reson*, 2017, **284**, 1-7.
21. S. J. DeVience, R. L. Walsworth and M. S. Rosen, *Phys Rev Lett*, 2013, **111**, 173002.
22. A. N. Pravdivtsev, A. S. Kiryutin, A. V. Yurkovskaya, H. M. Vieth and K. L. Ivanov, *J Magn Reson*, 2016, **273**, 56-64.
23. B. A. Rodin, A. S. Kiryutin, A. V. Yurkovskaya, K. L. Ivanov, S. Yamamoto, K. Sato and T. Takui, *J Magn Reson*, 2018, **291**, 14-22.
24. R. Buratto, D. Mammoli, E. Canet and G. Bodenhausen, *J Med Chem*, 2016, **59**, 1960-1966.
25. M. P. A. Fisher, *Annals of Physics*, 2015, **362**, 593-602.
26. Y. Feng, R. M. Davis and W. S. Warren, *Nat Phys*, 2012, **8**, 831-837.
27. G. Stevanato, S. S. Roy, J. Hill-Cousins, I. Kuprov, L. J. Brown, R. C. Brown, G. Pileio and M. H. Levitt, *Phys Chem Chem Phys*, 2015, **17**, 5913-5922.
28. M. C. Tayler and M. H. Levitt, *J Am Chem Soc*, 2013, **135**, 2120-2123.
29. H. J. Hogben, M. Krzystyniak, G. T. Charnock, P. J. Hore and I. Kuprov, *J Magn Reson*, 2011, **208**, 179-194.
30. C. Bengs and M. H. Levitt, *Magn Reson Chem*, 2018, **56**, 374-414.
31. R. Radeglia, *Solid State Nucl Magn Reson*, 1995, **4**, 317-321.
32. R. P. Young, C. R. Lewis, C. Yang, L. Wang, J. K. Harper and L. J. Mueller, *Magn Reson Chem*, 2019, **57**, 211-223.
33. W. Humphrey, A. Dalke and K. Schulten, *J Mol Graph*, 1996, **14**, 33-38, 27-38.
34. D. A. Case, I. Y. Ben-Shalom, S. R. Brozell, D. S. Cerutti, T. E. Cheatham III, V. W. D. Cruzeiro, T. A. Darden, R. E. Duke, D. Ghoreishi, G. Giambasu, T. Giese, M. K. Gilson, H. Gohlke, A. W. Goetz, D. Greene, R. Harris, N. Homeyer, Y. Huang, S. Izadi, A. Kovalenko, R. Krasny, T. Kurtzman, T. S. Lee, S. LeGrand, P. Li, C. Lin, J. Liu, T. Luchko, R. Luo, V. Man, D. J. Mermelstein, K. M. Merz, Y. Miao, G. Monard, C. Nguyen, H. Nguyen, A. Onufriev, F. Pan, R. Qi, D. R. Roe, A. Roitberg, C. Sagui, S. Schott-Verdugo, J. Shen, C. L. Simmerling, J. Smith, J. Swails, R. C. Walker, J. Wang, H. Wei, L. Wilson, R. M. Wolf, X. Wu, L. Xiao, Y. Xiong, D. M. York and P. A. Kollman, University of California, San Francisco2019.
35. N. Michaud-Agrawal, E. J. Denning, T. B. Woolf and O. Beckstein, *J Comput Chem*, 2011, **32**, 2319-2327.
36. R. Paquin, P. Pelupessy, L. Duma, C. Gervais and G. Bodenhausen, *J Chem Phys*, 2010, **133**, 034506.
37. G. Pileio, J. T. Hill-Cousins, S. Mitchell, I. Kuprov, L. J. Brown, R. C. Brown and M. H. Levitt, *J Am Chem Soc*, 2012, **134**, 17494-17497.
38. K. F. Sheberstov, H. M. Vieth, H. Zimmermann, B. A. Rodin, K. L. Ivanov, A. S. Kiryutin and A. V. Yurkovskaya, *Sci Rep*, 2019, **9**, 20161.
39. C. Bengs, L. Dagys, G. A. I. Moustafa, J. W. Whipham, M. Sabba, A. S. Kiryutin, K. L. Ivanov and M. H. Levitt, *ChemRxiv*, 2021, DOI: 10.33774/chemrxiv-2021-vlbbj.